Parameter Sensitivity of Primitive Equation Ocean General Circulation Models

FRANK BRYAN

National Center for Atmospheric Research, Boulder, CO 80307*

(Manuscript received 28 May 1986, in final form 11 December 1986)

ABSTRACT

Experiments with a low resolution, primitive equation ocean general circulation model with idealized basin geometry and surface forcing have been carried out in order to identify the processes controlling the climatically important aspects of the circulation. Emphasis was placed on the sensitivity of the model solutions to the magnitude of the vertical diffusivity. Scaling arguments suggest, and the numerical experiments confirm, that the solutions are most sensitive to the magnitudes of the wind stress curl and the vertical diffusivity. For small vertical diffusivity, wind forcing dominates the solution. The vertical scale of the thermocline is set by the strength of the Ekman pumping, and there is a multiple gyre circulation in the upper layers. For large vertical diffusivity, diabatic surface forcing dominates the solution. Vertical diffusion controls the vertical scale of the thermocline, and there is a single large anticyclonic gyre in the upper layers. Both the meridionally and zonally integrated overturning circulations are sensitive to the vertical diffusivity, though not to the same degree. The poleward heat transport is dominated by the zonally integrated meridional overturning circulation and, hence, also shows a sensitivity to the vertical diffusivity. The maximum poleward heat transport for the model used in this study varies by an order of magnitude as the vertical diffusivity is varied over a range comparable to that of estimates based on observations. The sensitivity to the prescription of the surface diabatic forcing and to other closure parameters is also described.

1. Introduction

The physical processes involved in the thermohaline-driven circulation are very poorly understood, yet are of great importance in questions of climate sensitivity and variability. Primitive equation ocean general circulation models (OGCMs) are one of the few tools currently available for studying the thermohaline circulation. In this study, the sensitivity of the climatically important properties (surface heat flux, poleward heat transport, water mass formation, etc . . .) of OGCMs to changes in closure parameters and surface diabatic boundary condition specification are determined by examining a series of solutions which span a broad range of parameter space. In addition to providing insight into the fundamental dynamics of the thermohaline circulation, these results give an indication of the reliability of numerical model results and those aspects of the model that will most profitably benefit from further developmental efforts.

The model used in this study is described in section 2. The philosophy adopted in its implementation was to retain the most general dynamical and physical processes of realistic OGCMs, but to use a relatively simple basin geometry and surface forcing distributions. The resolution is typical of that used in world ocean and coupled ocean–atmosphere models, and does not resolve mesoscale eddy processes. The result is a model that is economical to run, so that a large number of experiments can be integrated to equilibrium, yet the sensitivity should reflect that of larger models.

Preliminary estimates of the model sensitivity based on scaling arguments, are presented in section 3. They indicate that the model should be most sensitive to the magnitudes of the wind stress curl and the vertical diffusivity. Since the sensitivity of very similar models to variations in wind stress strength has been considered elsewhere (Bryan and Cox, 1967; Cox and Bryan, 1984), the emphasis in this study is placed on the role of vertical diffusion. While previous authors (Bryan and Lewis, 1979; Meehl et al., 1982) have carried out extensive parameter sensitivity studies with primitive equation models, there has been little discussion of the role of vertical diffusion. Further, these experiments were generally not integrated to equilibrium and did not resolve the long thermal response time scale of the deep ocean. In section 4, a series of experiments in which the vertical diffusivity was varied over a range comparable to that of estimates based on observations [$(0.1 \text{ to } 5.0) \times 10^{-4}$ m^2 s^{-1}] are described. The numerical results agree with the estimates of the sensitivity to this parameter based on scaling arguments.

Additional experiments in which the form of the surface diabatic boundary conditions or other closure parameters are varied, have also been carried out and are described in sections 5 and 6. A summary of the

* The National Center for Atmospheric Research is sponsored by the National Science Foundation.

parameter values used in each of the experiments is given in Table 1.

2. Description of the model

This section gives a cursory description of the model and the features unique to this study. For a more comprehensive discussion, the reader is referred to the technical reports of Semtner (1974) and Cox (1984).

The model is based on the primitive equations cast in spherical coordinates (λ, ϕ, z), where λ is longitude, ϕ is latitude, and z is height relative to the earth's mean radius, a (measured positive upwards). The model domain is a 60° wide sector of the sphere, extending from equator to pole, with a constant depth of 5000 m.

The equations of the model (the notation is standard) are given by

$$u_t + \mathcal{L}(u) - (f + u\tan\phi/a)v = -(1/a\cos\phi)(p/\rho_0)_\lambda + A_{MV}u_{zz} + F^\lambda \quad (1a)$$

$$v_t + \mathcal{L}(v) + (f + u\tan\phi/a)u = -(1/a)(p/\rho_0)_\phi + A_{MV}v_{zz} + F^\phi \quad (1b)$$

$$p_z = -\rho g \quad (1c)$$

$$T_t + \mathcal{L}(T) = A_{HV}T_{zz} + A_{HH}\nabla^2 T + CA(T) \quad (1d)$$

$$S_t + \mathcal{L}(S) = A_{HV}S_{zz} + A_{HH}\nabla^2 S + CA(S) \quad (1e)$$

$$\rho = \rho(S, T, p) \quad (1f)$$

$$(1/a\cos\phi)[u_\lambda + (v\cos\phi)_\phi] + w_z = 0. \quad (1g)$$

Here,

$$f = 2\Omega\sin\phi \quad (2)$$

is the Coriolis parameter, F^λ and F^ϕ represent the effect of horizontal eddy stresses.

$$F^\lambda = A_{MH}[\nabla^2 u + (1 - \tan^2\phi)u/a^2 - (2\tan\phi/a^2\cos\phi)v_\lambda] \quad (3a)$$

$$F^\phi = A_{MH}[\nabla^2 v + (1 - \tan^2\phi)v/a^2 + (2\tan\phi/a^2\cos\phi)u_\lambda] \quad (3b)$$

$\mathcal{L}(\ )$ denotes the advection operator,

$$\mathcal{L}(\sigma) = (1/a\cos\phi)[(u\sigma)_\lambda + (v\sigma\cos\phi)_\phi] + (w\sigma)_z \quad (4)$$

and the horizontal Laplacian ∇^2 is given by

$$\nabla^2\sigma = (1/a^2\cos^2\phi)[\sigma_{\lambda\lambda} + \cos\phi(\cos\phi\sigma_\phi)_\phi]; \quad (5)$$

A_{MH}, A_{HH}, A_{MV} and A_{HV} are the lateral eddy viscosity, lateral eddy diffusivity, vertical eddy viscosity and vertical eddy diffusivity, respectively. The term CA in the heat and salt equations schematically represents convective adjustment. The model cannot explicitly treat gravitational instabilities, so an implicit convection scheme is used. When the model predicts a statically stable stratification it has no effect, but when a gravitational instability is predicted, the water column is mixed vertically until stability is restored. The polynomial equation of state of Bryan and Cox (1972) is used for (1f).

The east and west walls of the basin are insulating, nonslip, impermeable boundaries:

$$u = v = T_\lambda = S_\lambda = 0. \quad (6)$$

At the equator a symmetry condition is applied:

$$u_\phi = v = T_\phi = S_\phi = 0. \quad (7)$$

Note that there is no northern boundary, as the basin extends to the pole. The bottom is taken to be insulating, free-slip, and impermeable:

$$u_z = v_z = w = T_z = S_z = 0. \quad (8)$$

The surface boundary conditions for temperature and salinity can be written as

$$A_{HV}(T, S)_z = (Q^T, Q^S), \quad (9a, b)$$

where the fluxes of temperature Q^T and salt Q^S may

TABLE 1. Summary of parameter values used in the sensitivity experiments. Entries are made only where the values differ from the reference case (experiment 1). A_{MH}: Horizontal viscosity, A_{MV}: Vertical viscosity, A_{HH}: Horizontal diffusivity, A_{HV}: Vertical diffusivity, τ_R: Restoration time scale for surface thermal boundary condition.

Experiment	A_{MH} ($m^2\ s^{-1}$)	A_{MV} ($m^2\ s^{-1}$)	A_{HH} ($m^2\ s^{-1}$)	A_{HV} ($m^2\ s^{-1}$)	τ_R (days)	Length of integration (years)
1	2.5×10^9	1.0×10^{-4}	1.0×10^7	0.5×10^{-4}	25	1172
2				0.1×10^{-4}		800
3				1.0×10^{-4}		1028
4				2.5×10^{-4}		787
5				5.0×10^{-4}		821
6					90	1025
7				2.5×10^{-4}	90	821
8				0.1×10^{-4}	*	821
9				2.5×10^{-4}	*	821
10			0.2×10^7			821
11			5.0×10^7			821

* Flux boundary condition used.

take one of two forms. In the reference case, and most of the sensitivity studies a linear damping condition is used for both temperature and salt,

$$Q^T = \Delta z_1(T^*(\phi) - T_1)/\tau_R \tag{10a}$$

$$Q^S = \Delta z_1(S^*(\phi) - S_1)/\tau_R \tag{10b}$$

where Δz_1 is the thickness of the uppermost model level, τ_R is the damping time constant, $T^*(\phi)$ and $S^*(\phi)$ are the reference temperature and salinity, and T_1 and S_1 are the temperature and salinity of the uppermost model level. For $T^*(\phi)$ and $S^*(\phi)$, observed (Levitus, 1982) zonally-annually averaged sea surface temperatures and salinities, composited from both hemispheres are used. In addition, the profiles (Fig. 1) have been slightly smoothed.

The second form which the surface thermal and salinity boundary conditions may take is a specified flux. The flux fields used in Experiments 8 and 9 were obtained by computing the surface fluxes implied by an equilibrium solution of the model obtained with linear damping conditions. These will generally be functions of longitude as well as latitude.

The wind stress applied to the surface has only a zonal component, and is a function only of latitude,

$$A_{MV}(u, v)_z = (\tau^\lambda, 0)/\rho_0. \tag{11}$$

The wind stress profile (Fig. 1) used in this study is given by a simple analytic expression that captures the major features of the observed zonally averaged zonal wind stress.

A rigid lid condition is used for vertical velocity at the surface,

$$w = 0. \tag{12}$$

The method of Bryan (1969) is used to integrate the model equations. The details of the finite difference equations and the proofs of their conservative properties may be found in Bryan (1969), Semtner (1974), and Cox (1984). The horizontal resolution is 3.75° longitude and 4.5° latitude. There are 12 levels in the vertical, with resolution varying from 50 m near the surface to about 850 m near the bottom. The method described by Bryan (1984) for accelerating the convergence of the model, in which the momentum and thermodynamic equations are integrated asynchronously, was used in all the experiments.

While the latitude–longitude configuration of the model finite difference grid simplifies the equations and has been shown to have certain computational advantages (Holloway et al., 1973), the convergence of meridians near the pole places a severe restriction on the length of the time step allowed for computational stability. This restriction is overcome by Fourier filtering the prognostic fields in the zonal direction in order to suppress the shortest wavelength components. The technique used is based on that of Bryan et al. (1975). In the initial configuration of the model, all prognostic variables were filtered poleward of 45°. It was found, however, that filtering the horizontal velocity components introduced large amplitude noise in the vertical velocity field in the form of alternating cells of upward and downward motion, the number of cells being just equal to the number of harmonics retained in the Fourier recomposition. This is easy to understand, as the truncated expansion of an initially nondivergent horizontal velocity field need not be nondivergent. To supress these undesirable side effects, the velocity was filtered only poleward of 80° latitude. While this did not eliminate the problem, it did relegate it to a rather quiescent region of the basin that did not strongly affect the rest of the solution.

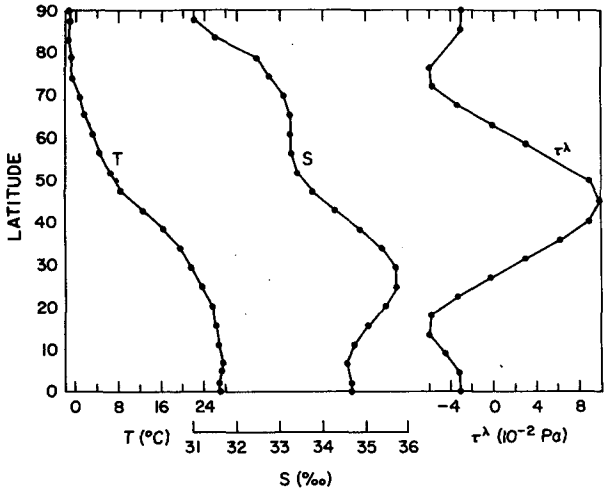

FIG. 1. Surface boundary conditions. Temperature and salinity profiles used in Newtonian damping condition (T and S) and surface wind stress ($\tau\lambda$).

3. Preliminary considerations

Before examining the results of the general circulation model it is useful to make some preliminary estimates of the response to changes in the model parameters. We do this by considering some simple scaling relationships for the velocity and thermal fields based on classical thermocline theory (Veronis, 1969; Welander, 1971). We scale the model equations for flow characterized by geostrophic–hydrostatic balance:

$$(u_*, v_*, w_*) = U(u, v, Dw/a) \tag{13a}$$

$$p_* = 2\Omega U a \rho_0 p \tag{13b}$$

$$\rho_* = \rho_0(2\Omega U a/gD)\rho, \tag{13c}$$

where the asterisk subscript denotes a dimensional quantity, U is the characteristic horizontal velocity scale and D is the depth scale of the motion. Estimates of these scales may be obtained from the imposed boundary conditions and the model parameters. If the vertical

velocity is scaled by the magnitude of the Ekman pumping,

$$W_e = \Delta\tau/\rho_0 2\Omega a \tag{14}$$

where $\Delta\tau$ is a measure of the range of magnitude of the zonal wind stress, we obtain a horizontal velocity scaling corresponding to Sverdrup balance

$$U_s = W_e a/D = \Delta\tau/\rho_0 2\Omega D. \tag{15}$$

If we scale density variations by the range of density imposed at the surface $\Delta\rho^*$, then

$$\Delta\rho^*/\rho_0 = 2\Omega U a/gD = \Delta\tau a/\rho_0 g D^2. \tag{16}$$

This relation yields an "advective" depth scale D_a;

$$D_a = [(\Delta\tau/\rho_0)a/g(\Delta\rho^*/\rho_0)]^{1/2}, \tag{17}$$

and the associated "wind driven" velocity scale U_s;

$$U_s = [\Delta\tau g(\Delta\rho^*/\rho_0)/\rho_0 4\Omega^2 a]^{1/2}. \tag{18}$$

Alternatively, we can choose the advective–diffusive depth scale (e.g. Munk, 1966) as the appropriate vertical scaling:

$$D = A_{HV}/W = A_{HV}a/UD. \tag{19}$$

Utilizing the thermal wind scaling (13c) to eliminate U yields a "diffusive" depth scale D_d

$$D_d = [2\Omega a^2 A_{HV}/g(\Delta\rho^*/\rho_0)]^{1/3}. \tag{20}$$

Finally, substituting back into (13c) we get the "thermally driven" velocity scale U_t:

$$U_t = [(g\Delta\rho^*/2\Omega\rho_0)^2 A_{HV}/a]^{13}. \tag{21}$$

For the reference case $\Delta\tau/\rho_0 = 1.5 \times 10^{-4}$ m^2 s^{-2}, $\Delta\rho^*/\rho_0 = 4 \times 10^{-3}$, and $A_{HV} = 0.5 \times 10^{-4}$ m^2 s^{-1} yielding

$U_s = 0.7 \times 10^{-2}$ m s^{-1} $\quad U_t = 0.8 \times 10^{-2}$ m s^{-1}

$D_a = 156$ m $\quad D_d = 196$ m.

We see that for the reference case, the wind and buoyancy forcing result in velocities of equal magnitude. Further, the advective and diffusive thermocline scale depths are comparable. A useful measure of the relative strengths of the wind and thermal forcings is the ratio of the two velocity scales, γ:

$$\gamma = U_s/U_t.$$

Several previous studies have used these scalings or ones similar to them to characterize their experiments (e.g., Bryan and Cox, 1967, 1968; Gill and Bryan, 1971; Holland, 1971, 1975). Table 2 summarizes the velocity and depth scales, and the values of several nondimensional parameters for each experiment in the present study, as well as several of the studies cited previously. The flow in the experiments of this study is very viscous, which can be seen by comparing the Reynolds number (Table 2) with those in the previous studies. The relative strengths of the thermal and wind forcings are close to unity for all the experiments, however. For Experiments 2 and 1 [$A_{HV} = (0.1\text{–}0.5) \times 10^{-4}$ m^2 s^{-1}], the wind driven velocity scale slight exceeds the thermal velocity scale, while for Experiments 3–5 [$A_{HV} = (1.0\text{–}5.0) \times 10^{-4}$ m^2 s^{-1}], the thermal velocity scale exceeds the wind driven velocity scale. Only for Experiment 2 does the advective thermocline depth scale exceed the diffusive depth scale. Thus we can expect to see a transition in the behavior of the model between Experiments 1 and 2 and the rest of the experiments.

4. Sensitivity to vertical mixing

a. The reference solution

The reference case (Experiment 1) was started from a resting homogeneous state with a temperature of 5°C and salinity 33.0‰, and integrated forward in time for

TABLE 2. Velocity and depth scales, and nondimensional parameters for the experiments in this study and several previous studies.

Experiment	U_t (cm s^{-1})	U_s (cm s^{-1})	D_d (m)	D_a (m)	R_0 ($\times 10^{-5}$)	R_e	Ek_H ($\times 10^{-5}$)	Ek_V ($\times 10^{-5}$)	Re_H	Re_V	γ
1	0.7	0.8	196	156	0.8	0.2	4.2	1.8	44.5	0.8	1.1
2	0.5	0.8	115	156	0.5	0.1	4.2	5.1	31.8	2.1	1.6
3	1.1	0.8	247	156	1.2	0.3	4.2	1.1	70.0	1.0	0.7
4	1.5	0.8	335	156	1.6	0.4	4.2	0.6	95.5	0.7	0.5
5	1.9	0.8	422	156	2.0	0.5	4.2	0.4	121.0	0.6	0.4
6	0.7	0.8	196	156	0.8	0.2	4.2	1.8	44.5	0.8	1.1
7	1.5	0.8	335	156	1.6	0.4	4.2	0.6	95.5	0.7	0.5
8	*	0.8	*	*							
9	*	0.8	*	*							
10	0.7	0.8	196	156	0.8	0.2	4.2	1.8	89.0	0.8	1.1
11	0.7	0.8	196	156	0.8	0.2	4.2	1.8	222.5	0.8	1.1
Bryan and Cox (1968)					20.0	150.0	0.1	0.2	150.0	0.01	1.0
Gill and Bryan (1971)					200.0	22.0	9.0	2.4	32.0	0.01	1.1
Holland (1971)					1.5	1.8	8.0	0.004	18.0	0.002	3.4
Holland (1975) 1					1.5	0.9	1.7		90.0		3.4
Holland (1975) 2					1.5	1.8	0.8		18.0		0.0

* Fixed flux boundary conditions preclude a priori estimate.

nearly 1200 years. The solution at this stage will be referred to as the equilibrium solution, even though there were still some very slight trends in the thermal fields. The mean surface heat flux was -0.1 W m^{-2}, corresponding to a cooling of the basin mean temperature of 0.14°C per century. There were no discernible trends in the basin mean kinetic energy. Each of the sensitivity experiments was initialized with this reference equilibrium solution or that of another experiment which was parametrically closer. Since the emphasis of this study is the nature of the sensitivity of the equilibrium solutions rather than the adjustment processes leading to equilibrium, little analysis has been performed on the intermediate stages of the integrations.

The surface (25 m) temperature and salinity fields for Experiment 1 are shown in Fig. 2a–b. Over most of the interior of the basin, surface values are very close to their reference values $T^*(\phi)$ and $S^*(\phi)$, indicating that the surface advective and diffusive time scales in the interior of the basin are much longer than the 25 day restoring time scale of the boundary conditions.

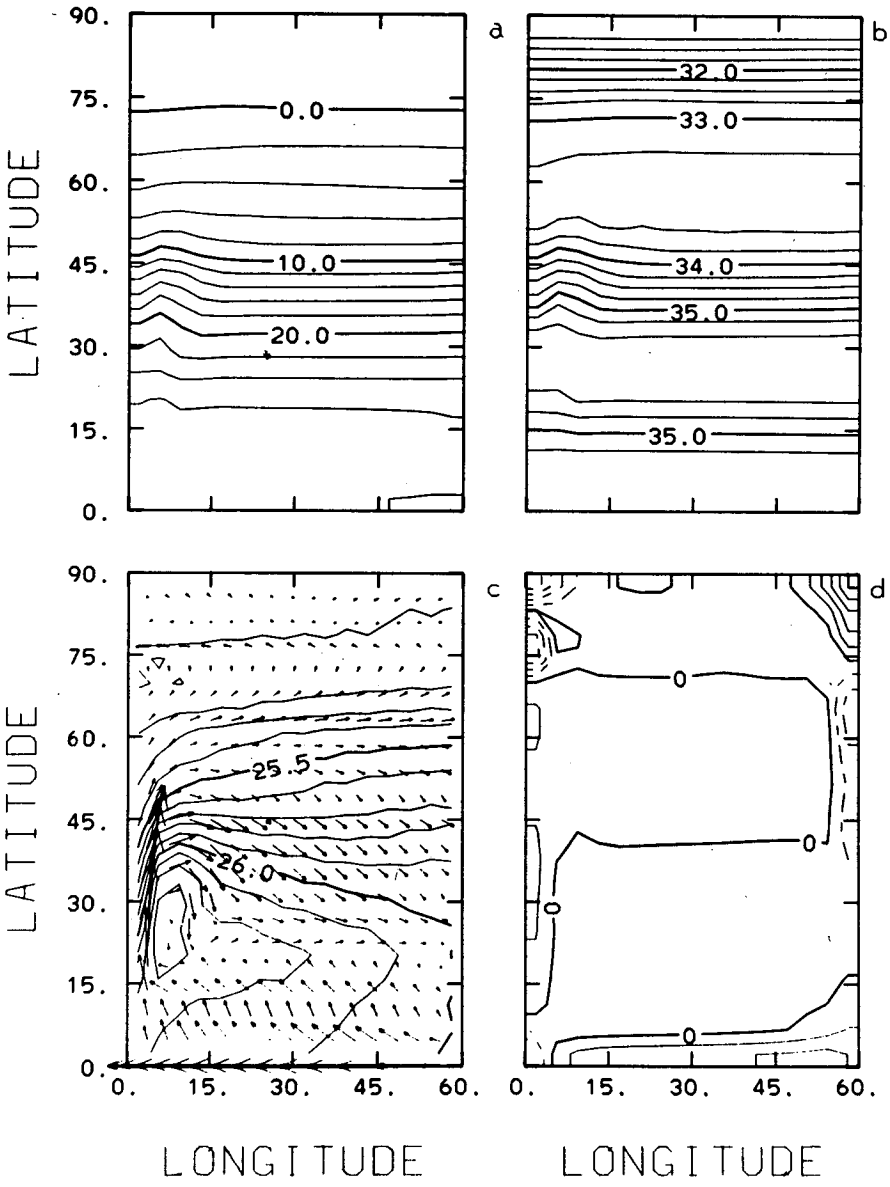

FIG. 2. Solution for Experiment 1 at 25 m. (a) Temperature (contour interval = 2°C), (b) Salinity (c.i. = 0.2‰), (c) Horizontal velocity (vector 1° long = 0.15 cm s^{-1}) and pressure (c.i. = 0.1 db), (d) Vertical velocity (c.i. = 2×10^{-4} cm s^{-1}).

In the western boundary layer and near the equator, advection is sufficiently strong to cause the surface values to deviate significantly from their reference values.

An important implication of the zonality in the surface temperature and salinity (and hence density) fields is that it will lead to a strong zonal-vertical circulation through the thermal wind relationship. The horizontal velocity field at 25 m is shown in Fig. 2c superimposed on the pressure distribution. The western boundary current has maximum velocities of about 0.15 m s^{-1}. This is an order of magnitude less than those observed in nature. The vertical velocity at the base of the surface layer (51 m) is shown in Fig. 2d. Except along the western and eastern boundaries, the vertical velocity is about equal to the Ekman pumping velocity. The downwelling along the eastern boundary, and upwelling along the western boundary are associated with the thermal wind field described above.

The thermocline for this solution is confined to the upper 500 m. Within this depth interval, the temperature and salinity fields show more east–west structure than at the surface, and the flow is very geostrophic. Below the thermocline, the water is nearly homogeneous with a temperature of about 1°C and salinity of 33‰.

b. Thermocline structure and circulation

While the water mass properties below the thermocline are very homogeneous and do not vary significantly among the experiments considered in this study, the depth and structure of the thermocline itself do change. The zonally averaged potential density in the upper 1000 m is shown in Fig. 3 for Experiments 2, 1, and 4 [A_{HV} = (0.1 to 2.5) × 10^{-4} m^2 s^{-1}]. As the vertical diffusivity increases, the thermocline deepens and thickens. This is just what is expected from the scaling considerations leading to (20). The deepening is strongest at lower latitudes, so the thermocline also becomes flatter at higher diffusivities, losing its bowl structure in the subtropics.

An *e*-folding depth for the potential density, z_e,

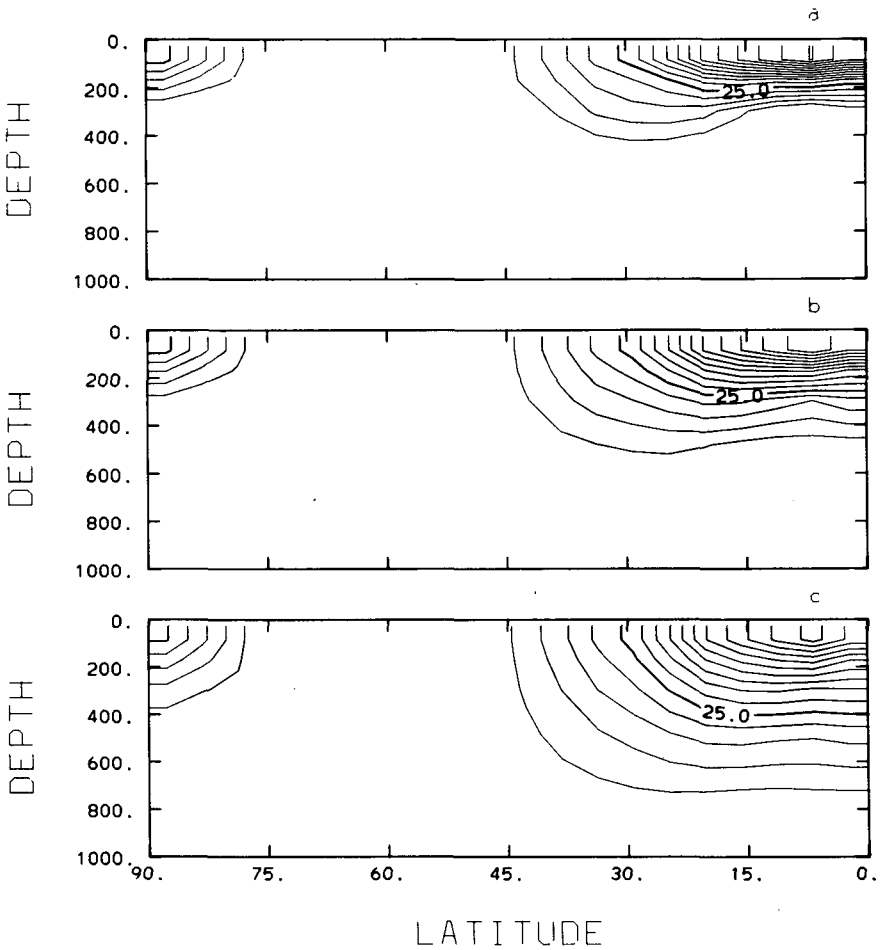

FIG. 3. Zonal average potential density in upper 1000 m for (a) A_{HV} = 0.1, (b) A_{HV} = 0.5, (c) A_{HV} = 2.5. (c.i. = 0.25 kg m^{-3}).

which we can identify as a scale depth for the thermocline, was computed at each location according to

$$\sigma_\theta(z_e) = \sigma_\theta(-H) + [\sigma_\theta(0) + \sigma_\theta(-H)]/e.$$

The zonally averaged scale depths are plotted as a function of A_{HV} for selected latitudes in Fig. 4. At higher diffusivities, scale depth increases as approximately the ⅓ power of A_{HV} as predicted by the scaling for D_d. At lower diffusivities (0.1×10^{-4} to 0.5×10^{-4} m^2 s^{-1}), however, the sensitivity is decreased. The advective scaling for the thermocline depth must come into play here, maintaining a minimum thermocline depth. Note that Experiment 2 ($A_{HV} = 0.1 \times 10^{-4}$ m^2 s^{-1}) is the only case with γ significantly greater than one, indicating a predominance of wind forcing over thermal forcing. The profile of the zonally averaged thermocline depth was also qualitatively different in the subpolar gyre region for this case compared to the other cases, showing a doming of the thermocline in response to the Ekman suction.

Since the momentum balances in the model are highly geostrophic, we can expect the changes in the thermocline shape to be reflected in the circulation. The horizontal velocity fields near the surface for Experiments 2 (low vertical diffusivity) and 4 (high vertical diffusivity) are shown in Figs. 5b and 6b. In the low mixing case, the western boundary current separates from the coast near the zero wind stress curl line, and a weak but still distinct subpolar gyre is present. In the high mixing case, the western boundary current is much stronger and penetrates to higher latitudes. The interior circulation in the high mixing case is also very zonal and there is no evidence of a subpolar gyre. These changes can be understood in terms of the changes in the topography of the thermocline discussed above.

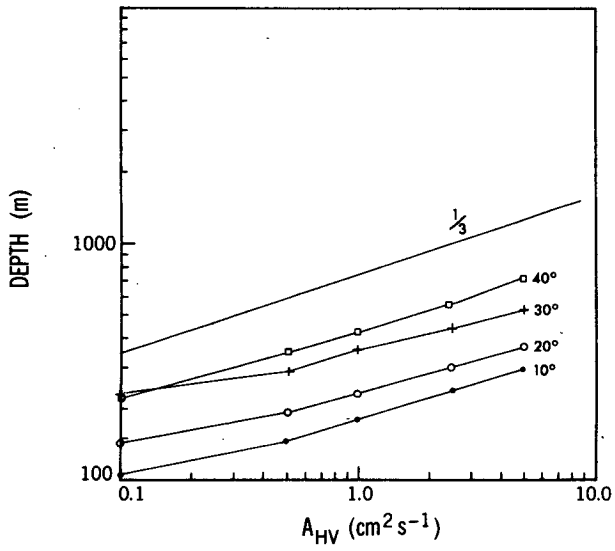

FIG. 4. Dependence of thermocline e-folding scale depth on vertical diffusivity at selected latitudes.

Since the latitude of density surface outcrops are closely constrained by the surface boundary conditions, the deepening of the subtropical and tropical thermocline results in an increase in the mean meridional slope of isopycnal surfaces. This implies that the vertical shear of the zonal current must increase by the thermal wind relationship. Since the meridional buoyancy gradient has the same sign over most of the basin and is nearly zonally symmetric, the thermally induced flow will be eastward in the surface layers and nearly zonally symmetric. For the higher mixing cases, the shear is large enough to overcome the tendency of the wind forcing to form counterrotating gyres in the upper layers (note that the vertically integrated circulation is unchanged).

The changes in the strength of the western boundary current with increasing diffusivity lead to an increase in the degree of deviation of the isotherms and isohalines from their reference values in the western boundary region (Figs. 5a and 6a). We can anticipate that this will lead to significant changes in the surface heat and salt fluxes. The increased zonal circulation in the surface layers of the high diffusivity case is accompanied by an increase in the magnitude of the vertical velocity on the meridional boundaries to satisfy mass balance.

These changes in the surface circulation are very similar to changes in the solutions of Bryan and Cox (1967) and Cox and Bryan (1984) as the magnitude of the wind stress curl was varied. For a purely thermally driven circulation, they obtained a solution similar to the higher diffusivity cases with a single anticyclonic gyre with very zonal interior flow. As the wind stress was turned on, then doubled, the circulation took on a multiple gyre structure, similar to the lowest diffusivity case of the present study. Thus, increasing the magnitude of the vertical diffusivity has similar effects to decreasing the Ekman pumping. This relationship is embodied in the parameter γ, which is a function of both. For $\gamma > 1$, the wind driven circulation dominates, while for $\gamma < 1$, the thermally driven circulation dominates.

On the other hand, these results do not agree with previous estimates of the sensitivity of the circulation to changes in vertical diffusivity made from similarity type solutions to the classical thermocline equations (Alexander, 1971). These solutions respond to increased diffusivity with an increase in upwelling from depth, but little change in the horizontal structure of the circulation. This results from the use of a single scale factor in the exponential vertical structure of the solution, thus preventing changes in the mean meridional slope of the thermocline; as indicated previously, this is a key element in the sensitivity of the full three dimensional model.

c. *Integral circulations*

A streamfunction for the zonally integrated mass transport or "meridional overturning" circulation can be defined as

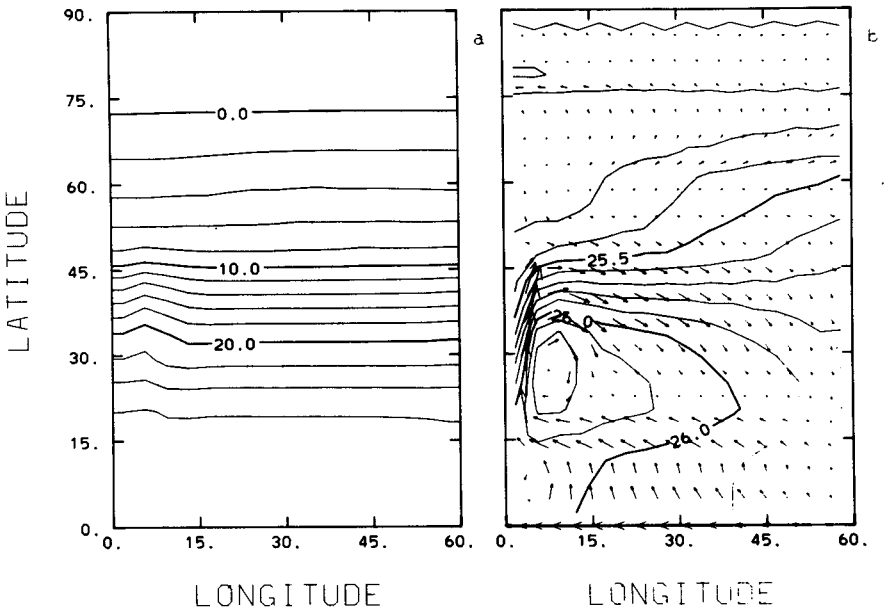

FIG. 5. Solution for Experiment 2 at 25 m. (a) Temperature (contour interval = 2°C), (b) Horizontal velocity (vector 1° long = 0.15 cm s^{-1}) and pressure (c.i. = 0.1 db).

$$\Phi_z = \int_{\lambda_w}^{\lambda_e} va \cos\phi d\lambda \tag{22a}$$

$$-a^{-1}\Phi_\phi = \int_{\lambda_w}^{\lambda_e} wa \cos\phi d\lambda, \tag{22b}$$

and is shown in Fig. 7 for Experiments 2, 1, and 4 [A_{HV} = (0.1, 0.5, and 2.5) × 10^{-4} m^2 s^{-1}, respectively]. The predominant feature is an overturning cell that increases in magnitude from about 7.5 × 10^6 to 30 × 10^6 m^3 s^{-1}. Deep water forms, and sinks near 70° latitude and upwells more or less uniformly over the remainder of the basin. A much shallower circulation driven by Ekman pumping is present near the equator. Deeper on the equator, there is a counterrotating cell that decreases in magnitude with increasing diffusivity and is absent in the higher diffusivity cases. Inspection of the vertical velocity fields shows that this cell is pri-

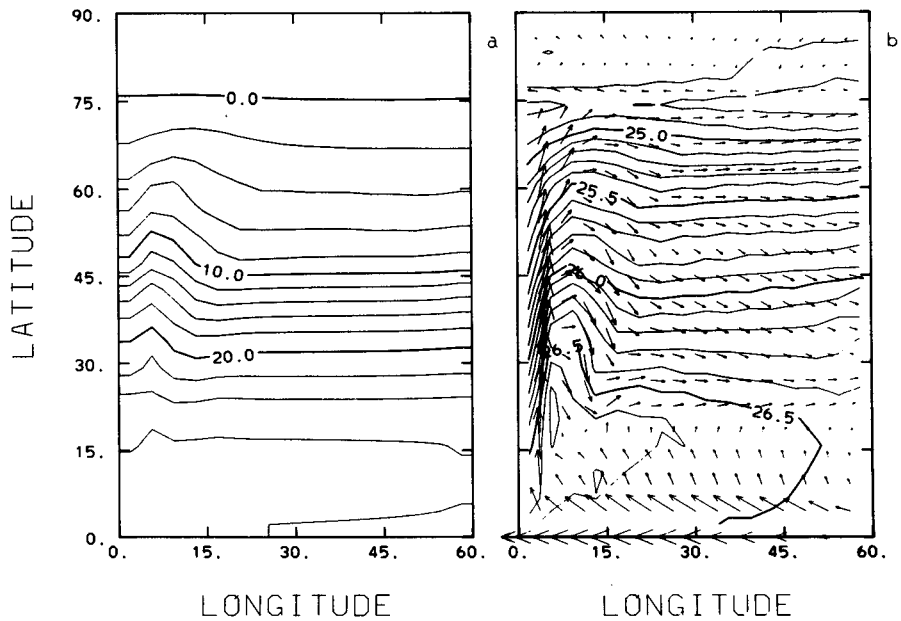

FIG. 6. As in Fig. 5 except for Experiment 4 (A_{HV} = 2.5 × 10^{-4} m^2 s^{-1}).

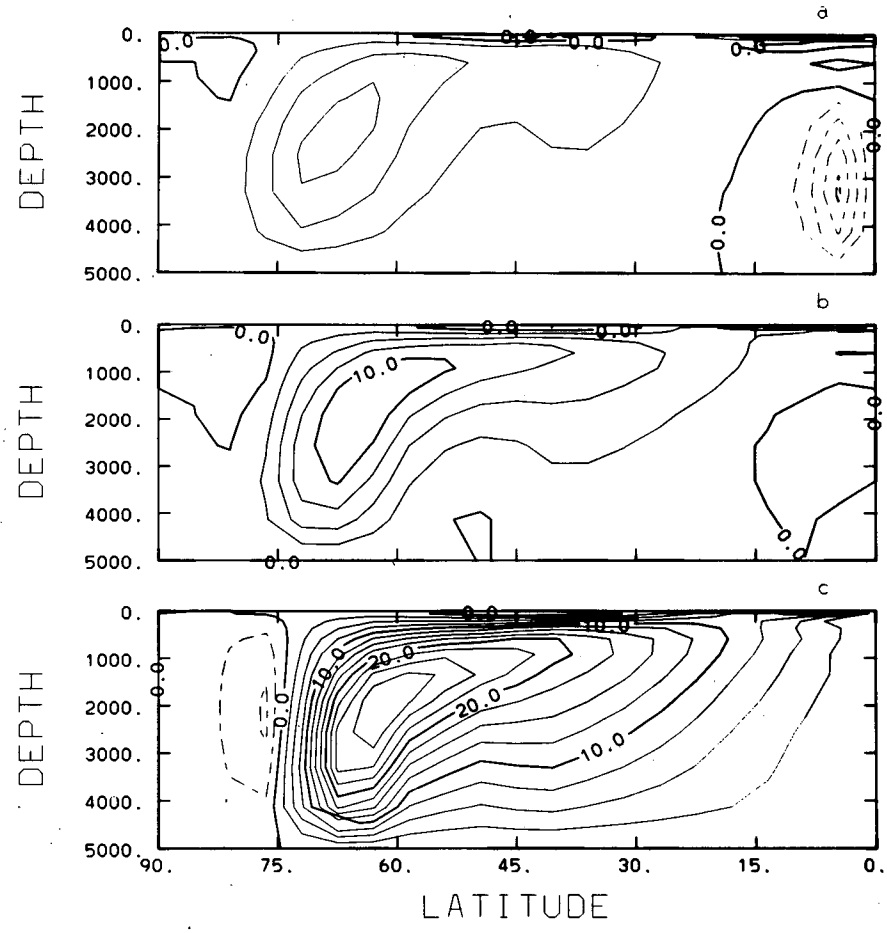

FIG. 7. Meridional overturning streamfunction for (a) $A_{HV} = 0.1$, (b) $A_{HV} = 0.5$, (c) $A_{HV} = 2.5$ (c.i. = 2.5×10^6 m^3 s^{-1}, solid contours indicate counterclockwise circulation).

marily due to downwelling on the eastern boundary at the equator. The physical processes driving this circulation are difficult to determine and need further study. Similar features are present in the models of Takano (1981) and Cox and Bryan (1984). Cox and Bryan attribute it to unspecified numerical difficulties. The dependence of the strength of the primary meridional overturning cell on the magnitude of the vertical diffusivity is shown in Fig. 8. The overturning shows an approximately cube root dependence on the diffusivity.

In an analogous manner, we can integrate the continuity equation meridionally, and define a zonal–vertical plane mass transport streamfunction. This quantity is plotted for Experiments 2, 1 and 4 in Fig. 9. The changes in the surface circulation patterns discussed above are very visible here. The increased zonal flow at high diffusivity leads to a much stronger zonal overturning circulation. Further, the upper branch of the circulation extends to greater depth in the high diffusivity case. The dependence of the primary zonal overturning cell on the diffusivity is shown in Fig. 10, in-

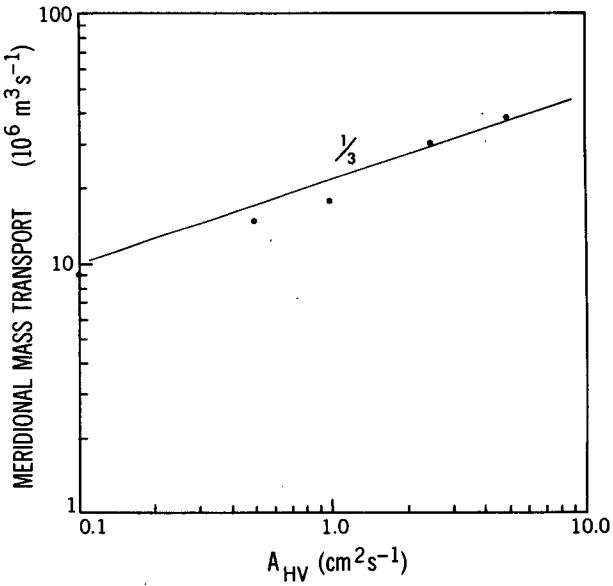

FIG. 8. Dependence of meridional overturning streamfunction on vertical diffusivity.

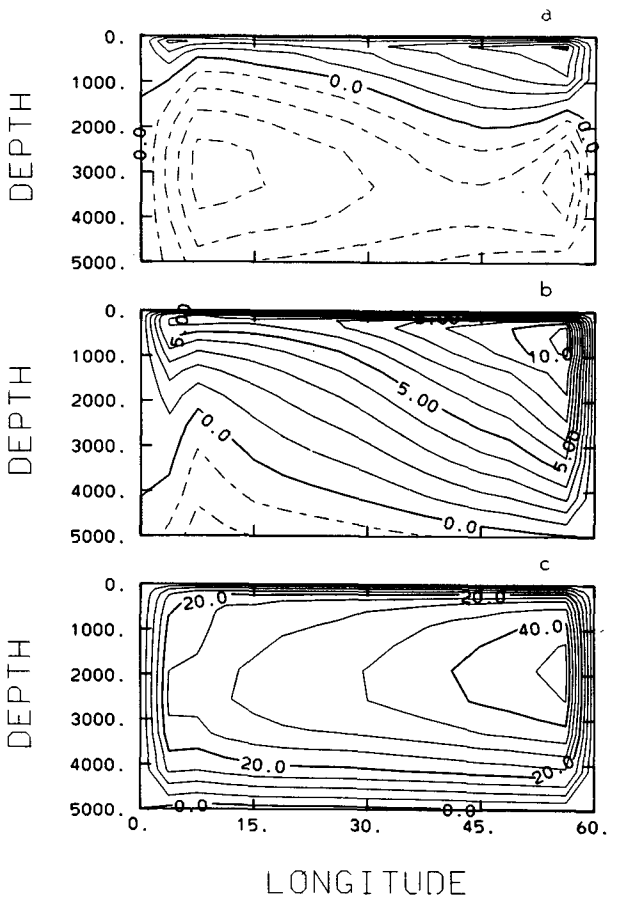

FIG. 9. Zonal overturning streamfunction for (a) A_{HV} = 0.1, (b) A_{HV} = 0.5, (c) A_{HV} = 2.5 [c.i. = 1 × 10^6 m^3 s^{-1} for (a) and (b), 5 × 10^6 m^3 s^{-1} for (c), solid contours indicate clockwise circulation].

dicating a ⅔ power dependence. This agrees with the diffusive scaling relationships, since the mass transport should be proportional to the product of U_t and D_d, which both have cube root dependence on A_{HV}. Apparently, the meridional overturning does not follow the same scaling and is not quite as sensitive to the magnitude of the diffusivity. Previous authors (Bryan and Cox, 1967) have not made this distinction, and a physical basis for the ⅓ power dependence of the meridional overturning remains to be found.

d. *Energetics*

The basin mean kinetic energy equation is

$$\langle u^2+v^2\rangle_t = -\langle \rho g w\rangle + H^{-1}\overline{u_s \tau^\lambda} - \rho_0 A_{MV}\langle u_z{}^2+v_z{}^2\rangle + \rho_0\langle uF^\lambda + vF^\phi\rangle \quad (23)$$

where $\langle(\ )\rangle$ represents a basin volume mean, $\overline{(\ )}$ represents a mean over the horizontal area of the basin, and u_s is the zonal component of the surface velocity. In deriving the potential energy equation, we make the simplifying assumption that the density obeys the same conservation equation and boundary conditions as do the temperature and salinity individually. This is not strictly true, due to the nonlinearity of the equation of state. The resulting equation for the basin mean potential energy is

$$\langle \rho g z'\rangle_t = \langle \rho g w\rangle - \overline{gQ} - gA_{HV}(\bar{\rho}_s - \bar{\rho}_B)/H + \langle CAgz'\rangle. \quad (24)$$

It is sometimes useful to consider the available potential energy, instead of the full potential energy. An estimate, which is adequate for the purposes of this study, is given by

$$\langle \mathrm{APE}\rangle = -\langle g\rho'^2/2(\partial\bar{\rho}/\partial z)\rangle. \quad (25)$$

In equilibrium, the left-hand sides of (23) and (24) vanish. Further, the mean surface heat flux $\bar{Q}$ must be identically equal to zero, so the second term on the right-hand side of (24) vanishes. A convenient way of presenting the terms in the equilibrium energy equations is as an energy cycle block diagram as depicted schematically at the top of Fig. 11. The energy cycles for Experiments 1–4 are presented in the same figure.

As the vertical diffusivity increases, the available potential energy (APE) increases. Once again, the changes in the shape of the thermocline enter into the problem. The increase in the mean meridional slope of isopycnal surfaces causes the variance of density on a level surface, ρ'^2 to increase. The overall thickening of the thermocline results in a slight decrease in the mean stratification $\bar{\rho}_z$. Both of these effects contribute to an increase in the APE.

The total potential energy $\langle P\rangle$ is many orders of magnitude greater than the APE, and is almost entirely associated with the stratification of the level mean state.

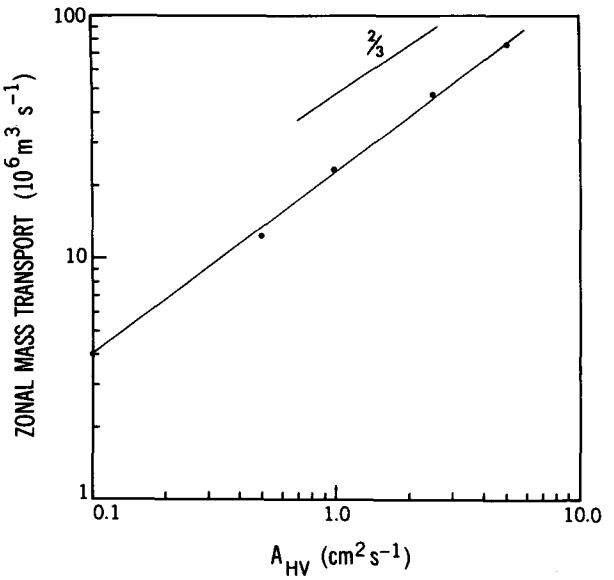

FIG. 10. Dependence of zonal overturning streamfunction on vertical diffusivity.

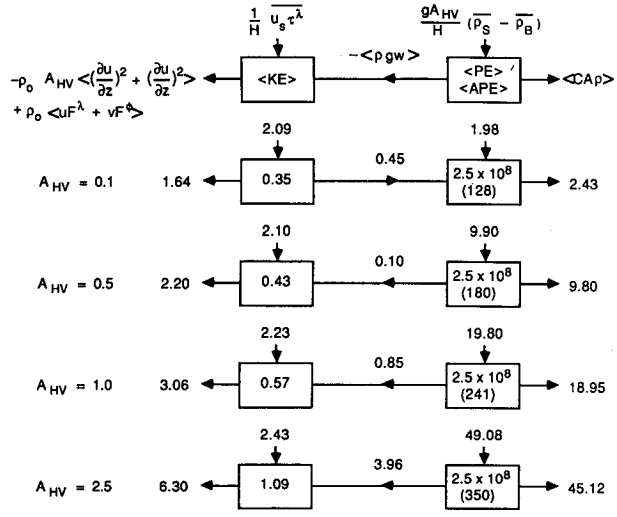

FIG. 11. Equilibrium energy cycle block diagram schematic (top), and energy cycles for experiments 1–4.

The generation of potential energy is seen to increase in direct proportion to the vertical diffusivity. Since the deep water density and the mean surface density are nearly constant for all the experiments, the top-to-bottom stratification $\bar{\rho}_s - \bar{\rho}_B$ is invariant to changes in vertical diffusivity. Thus, the generation term is simply linearly proportional to A_{HV}. A large fraction of the potential energy generation is directly compensated by dissipation by convection.

For the large scale ocean circulation, the available potential energy exceeds the kinetic energy by a factor approximately equal to the ratio of the basin scale to the internal radius of deformation (Gill et al., 1974). This is the case here with the ratio of APE to KE equal to 350–400. As the vertical diffusivity increases and the thermally forced circulation becomes stronger, the kinetic energy increases. Since the changes in the circulation in these experiments are thermally induced, the increase in kinetic energy must be supported by an increase in the buoyancy work. In the lowest diffusivity experiment, the sign of the buoyancy work is negative; i.e., there is a net conversion of kinetic to potential energy. For this case, the wind forcing is helping to maintain the thermocline structure. For the higher diffusivity cases the buoyancy work is positive and increases with increasing diffusivity; i.e., the thermal forcing is driving a more vigorous flow. The changes in the buoyancy work can be related to the changes in the integral circulations discussed in the previous section. The increase in the meridional overturning results in more cold water sinking, and more warm water rising, thereby increasing the correlation $-w'\rho'$. There is also a slight increase in the wind work as the diffusivity increases and the surface flow becomes stronger and more aligned with the wind stress.

Holland (1975) presented the energy cycles for two experiments in which the parameter γ was varied by changing the wind forcing. He obtained similar results to those here, with a net conversion of kinetic to potential energy for $\gamma > 1$, and vice versa for $\gamma < 1$. Thus, we again see that the character of the model solution depends strongly on this parameter.

e. *Surface heat fluxes and poleward heat transport*

As discussed above, the deviation of the surface temperature and salinity fields from their reference values in the western boundary region increases with increasing diffusivity and the strengthening of the boundary current. The surface heat fluxes thus increase in magnitude in this region (Figs. 12a–c). There are also qualitative changes in the pattern of the surface heat flux. In Experiment 2 there is a region of heat gain along the western boundary between 50° and 70° latitude, where the boundary current of the subpolar gyre flows equatorward. In contrast, the heat flux is out of the ocean everywhere poleward of 25° along the western boundary in the high diffusivity case. The pattern and magnitude of the surface salt flux undergoes similar changes and will not be discussed here.

A quantity of primary interest in studies of the ocean's role in the global climate system is the poleward heat transport. Numerical models provide one method for estimating these transports. There are considerable discrepancies between the estimates obtained from quite similar models (e.g., Bryan and Lewis, 1979 vs Meehl et al., 1982), however, and it is not clear how sensitive the computed transports are to various modeling assumptions.

The total northward heat transport through a zonal–vertical section extending across the entire basin from top to bottom is

$$F^H = HL\rho_0 c_p[\overline{vT - A_{HH}a^{-1}T_\phi}] \tag{26}$$

where $[(\ )]$ denotes a zonal average, $\overline{(\ )}$ a vertical average, and $L = a\cos\phi$. In order to aid the interpretation of the model results, it is useful to divide (26) into contributions due to various modes of the total circulation. Writing v and T in terms of their averages, and deviations therefrom, (4) becomes

$$F^H = HL\rho_0 c_p\{[\bar{v}][\bar{T}] + [\bar{v}^*\bar{T}^*] + \overline{[v'][T']} + \overline{[v'^*T'^*]} - A_{HH}a^{-1}[\bar{T}]_\phi\} \tag{27}$$

where $(\ )^*$ denotes a deviation from the zonal mean, and $(\ )'$ denotes a deviation from the vertical mean. For a basin with at least one closed zonal boundary, the net mass transport through any section $[v]$ must vanish, so the first term on the right-hand side of (29) is identically zero. The second term is associated with the vertically averaged barotropic circulation, the third with the zonally averaged meridional overturning circulation.

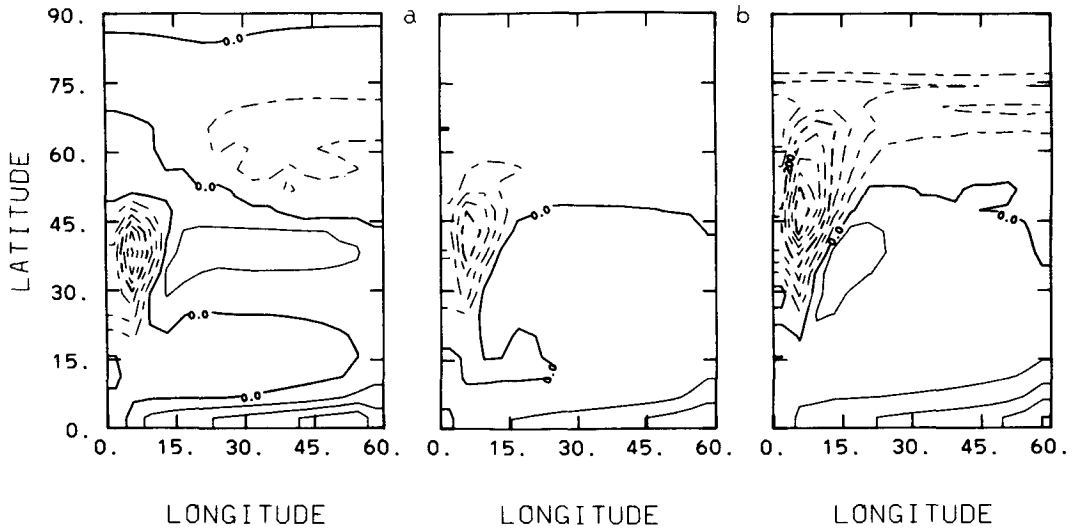

FIG. 12. Surface heat flux for (a) $A_{HV} = 0.1$, (b) $A_{HV} = 0.5$, (c) $A_{HV} = 2.5$ [c.i. = 25 W m^{-2} for (a), 50 W m^{-2} for (b) and (c)].

The components of the poleward heat transport are shown in Fig. 13 for the reference case. The meridional overturning is the dominant term at most latitudes. At low latitudes the shallow Ekman driven circulation makes the dominant contribution, while at mid- and high-latitudes the primary meridional overturning cell is dominant. The total transport is poleward everywhere with a maximum magnitude of about 0.4×10^{15} W. This is somewhat less than, but of the same order of magnitude, as estimates of the poleward heat transport in world ocean models.

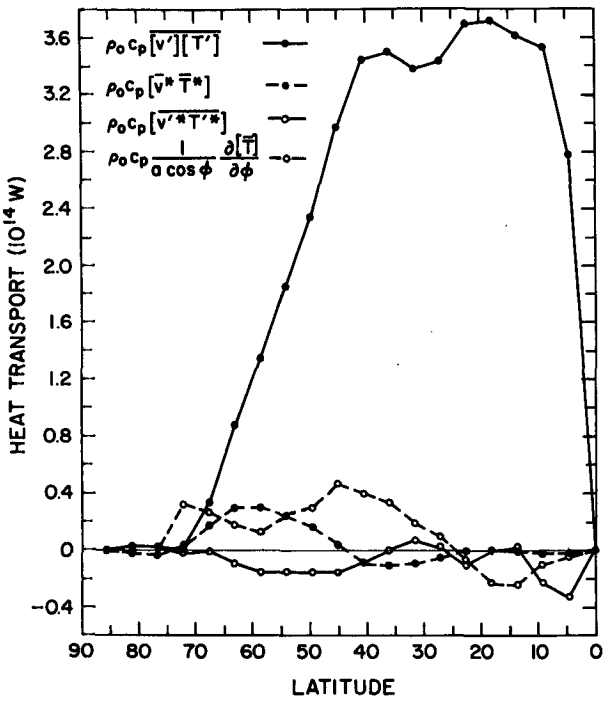

FIG. 13. Components of poleward heat transport for experiment 1.

As shown above, the meridional overturning is sensitive to the magnitude of the vertical diffusivity, so we can expect this sensitivity to extend to the poleward heat and salt transports. The total heat transports for Experiments 1–4 are shown in Fig. 14. For this range of the vertical diffusivity, the poleward heat transport increases by almost an order of magnitude. The differences between the heat transports obtained by Bryan and Lewis (1979) and Meehl et al. (1982), may be partially due to the differences in their choices of the magnitude of vertical diffusion. While Bryan and Lewis specified the vertical diffusivity as an increasing function of depth, its magnitude in the thermocline was between 0.3 and 0.5 ($\times 10^{-4}$ m^2 s^{-1}). Meehl et al. chose the vertical diffusivity as 10^{-4} m^2 s^{-1}, and obtained an annual average maximum poleward heat transport about 75% higher than Bryan and Lewis. As discussed by Meehl et al., differences in the specification of the surface wind stress may have also contributed to the differences in the heat transport results.

5. The role of surface thermal boundary conditions

a. Sensitivity to restoring time scale

In the previous section, the model solution changed both qualitatively and quantitatively in response to changes in the magnitude of the vertical diffusivity, and the sensitivity was well described by simple scaling relationships. To derive these scaling relationships the surface thermal boundary condition was treated as if a fixed meridional density gradient was imposed, rather than merely restoring towards one. Since the restoring time scale was sufficiently short to keep the surface

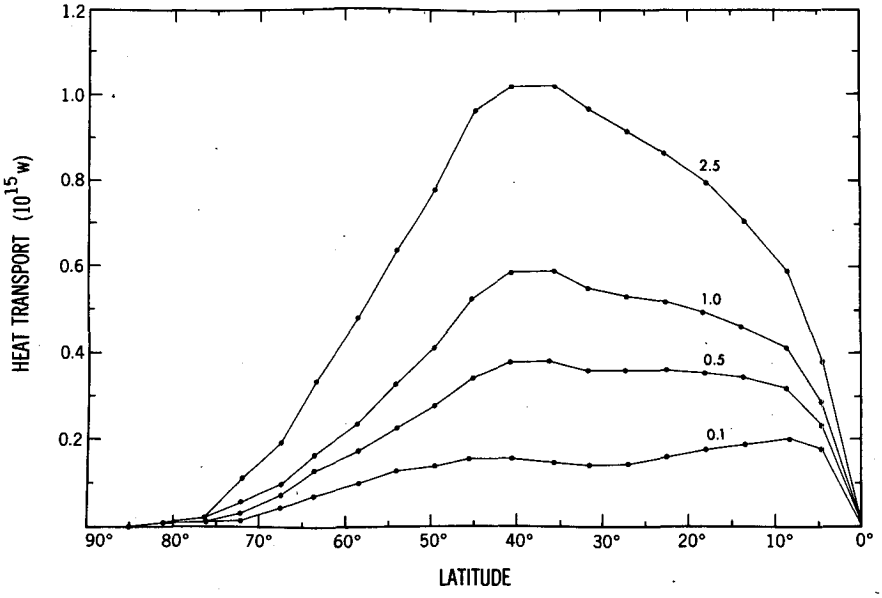

FIG. 14. Dependence of poleward heat transport on vertical diffusivity.

isopycnals close to their reference latitudes, this was a good approximation. It is of interest, however, to determine the sensitivity of the model solution and of the scaling relationships to the time scale used in the restoring boundary condition. In Experiments 6 and 7, this was done by increasing the time scale from 25 to 90 days.

The surface temperature distribution for Experiment 6 is shown in Fig. 15. The principle difference from the reference case is an increased displacement of isotherms from their reference positions, which, as discussed in the previous section, results in an increase in the magnitude of the surface heat flux. This case is somewhat different from the previous cases, however, in that compensating positive and negative displacements occur at the same latitude, so there is little change in the net surface heat flux at a particular latitude. Thus, the poleward heat transport is relatively insensitive to the change in τ_R.

There is little change in the horizontal or vertical velocity fields with increasing τ_R. At levels below the surface, the changes are quite small. There are apparent differences when integral circulations are considered however. The meridional overturning decreases in magnitude by about 30% with the increase in τ_R from 25 to 90 days, but the sensitivity to changes in A_{HV} remains the same. Cox and Bryan (1984) tested the sensitivity of their model to changes in this parameter, as well. They reported a decrease in convective activity as the time scale was increased.

b. *Sensitivity to vertical diffusivity with specified surface fluxes*

As shown in section 4, the magnitudes of the surface heat and salt fluxes increased with increasing diffusivity. In this sense, the diabatic forcing at the surface, as well as the internal diabatic forcing (through cross-isopycnal mixing), changed from one experiment to the next. To

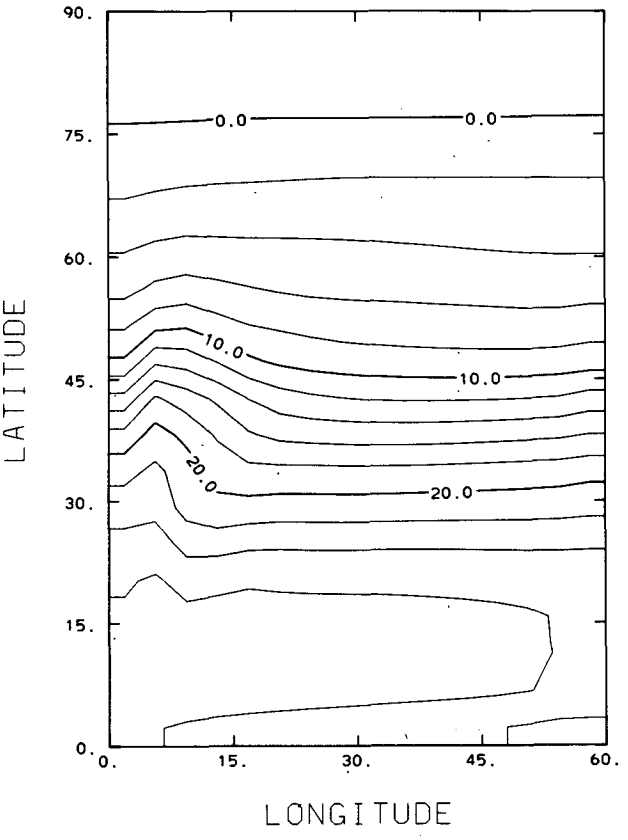

FIG. 15. Temperature at 25 m for experiment 6 (c.i. = 2°C).

try to isolate these two effects, another set of experiments (8–9) was carried out in which the vertical diffusivity was varied, but the surface fluxes were held constant and equal to those in the reference case.

With a fixed flux boundary condition, there is no longer a strict constraint on the range of surface temperature or salinity (though the basin mean values are constant). The equator to pole temperature difference exceeds 50°C for the low diffusivity case, while it is only about 15°C for the high diffusivity case. The enormous variability in Experiment 8 causes problems for the model because the equation of state employed is valid only inside a range of oceanographically relevant temperatures and salinities. We can still compare the response qualitatively, however. For both experiments, the surface thermal fields are much less zonal than in the corresponding cases with linear damping boundary conditions. The zonality of the surface flow at high latitudes in the high diffusivity case is also broken.

The changes in the structure of the thermocline in response to changes in vertical diffusivity when fixed flux boundary conditions are used are similar to those that occurred using restoring boundary conditions. The vertical scale of the thermocline decreases and the stratification increases with decreasing diffusivity. An exception is that the thermocline in the high diffusivity case has a stronger bowl-like structure than the lower diffusivity case.

The strength of the meridional overturning remains roughly the same for either type of boundary condition. Since the heat transport is fixed when the surface fluxes are specified, the sensitivity is not reflected in that quantity. An increase in the meridional overturning is compensated by a decrease in the vertical temperature differential to keep the poleward heat transport constant.

6. Sensitivity to other parameters

The magnitudes of the vertical diffusivity and the wind stress curl have been identified as controlling factors in the character of the model solution. These were the two quantities that arose naturally in the scale analysis of the model equations. The question remains as to whether any of the remaining closure parameters have as strong an influence on the model solutions. Holland (1975) identified a certain ratio of the horizontal diffusivity and horizontal viscosity as being important in determining the nature of the energy cycle. In order to compare the sensitivity of the model to this quantity and that described previously, two experiments were carried out in which the magnitude of the horizontal diffusivity was varied (Experiments 10 and 11).

The first notable effect of increasing the horizontal diffusivity is that the horizontal temperature and salinity fields are smoothed out. Zonal cross sections of temperature in the subtropical gyre region (Fig. 16) show that the warm core on the western boundary is considerably broadened. This is reflected in the surface circulation as a weakening of the boundary current and a nearly complete disappearance of the tight recirculation. Also, the western boundary current separates from the coast at a lower latitude and there is a more distinct subpolar gyre in the higher horizontal diffusivity case. Apparently the increase in horizontal diffusion has diminished the isopycnal slopes such that the wind forcing of the multiple gyre system becomes more pronounced.

In and below the thermocline there is an important difference in the vertical velocity distribution. While the vertical motion in the interior is primarily upward in the lower diffusivity case, there is a large region of downwelling in the western half of the basin at higher diffusivity. Veronis (1975) pointed out a similar feature in the model results of Holland (1971) and noted that large-scale downwelling in the interior was contrary to accepted ideas about the thermal balance of the abyssal ocean. He offered an explanation for the model results

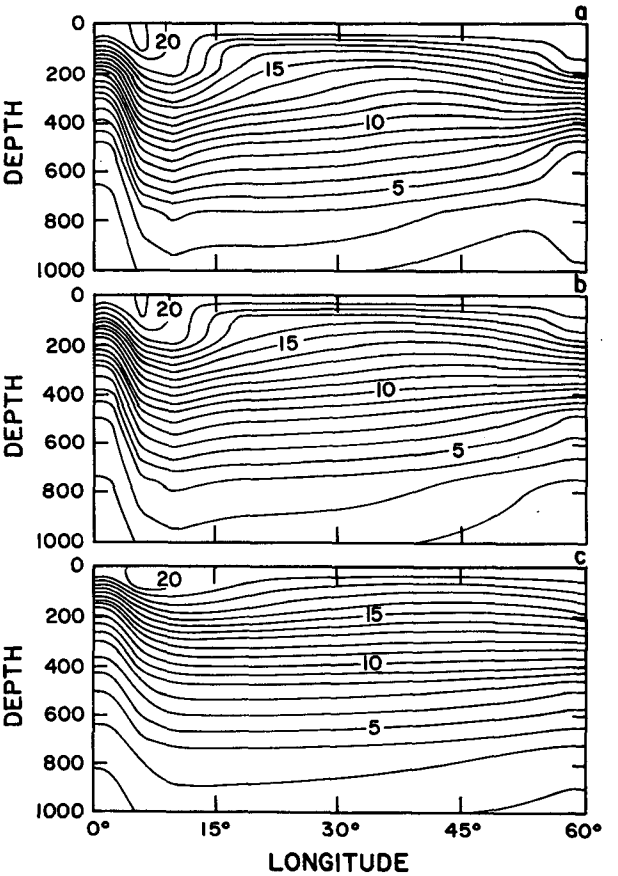

FIG. 16. Zonal temperature cross section in upper 1000 m for (a) $A_{HH} = 0.2 \times 10^7$, (b) $A_{HH} = 1.0 \times 10^7$, (c) $A_{HH} = 5.0 \times 10^7$, (c.i. = 1°C).

based on Holland's published figures that is substantiated quantitatively with the current model. In the western boundary region, warming of waters on the inshore side of the boundary current by horizontal diffusion is balanced primarily by upward advection of cold bottom water. As the horizontal diffusivity increases, the upwelling along the western boundary increases. When the western boundary upwelling becomes sufficiently strong, the deep water formation is insufficient to supply both the boundary upwelling and interior upwelling. Thus, water is forced to sink in the interior to satisfy mass balance for the deep ocean.

Changes in the horizontal diffusivity can result in some significant changes in the circulation, but not to the degree seen with changes in vertical diffusivity. The sensitivity to horizontal diffusivity results from its effect on cross isopycnal mixing. A reformulation of the model mixing parameterization in terms of isopycnal/diapycnal mixing coefficients would remove a large part of the sensitivity to this parameter.

A number of other experiments were carried out in which vertical viscosity was varied, or several parameters were varied in combination. Changes in vertical viscosity resulted in slight quantitative changes in regions of large vertical shears (especially the equator), but did not change the qualitative nature of the solution. Unfortunately, computational restrictions on the horizontal viscosity prevented direct testing of the sensitivity of the model to this parameter. Decreasing the viscosity can be expected to result in an increase in the strength of the time mean flow. The changes in the circulation resulting from changes in the ratio of the viscous and thermal boundary layers in the western boundary region, as described above, would occur in this case as well. Once the viscosity was decreased below some value however, barotropic and baroclinic instability would start to occur and eddies would begin to form. The role of eddies in the thermohaline circulation is beyond the scope of the current study.

7. Conclusions

This study considered the sensitivity of a numerical ocean general circulation model to changes in some of the closure parameters, with particular emphasis on the response of the thermohaline circulation. Sensitivity studies are a necessary and important part of the development of mathematical models of geophysical fluid systems. They can help to reveal aspects of the model that will most profitably benefit from further refinement, as well as to provide insights into the fundamental dynamics of these complicated fluid systems.

The primitive equation model used in the present study shows a great sensitivity to the magnitude of the vertical diffusivity. As the vertical diffusivity increases, the thermocline scale depth increases. This, in turn, results in an increase in the mean meridional slope of the thermocline, and hence the shear of the zonal current. The circulation thus becomes more zonal and intense with increasing diffusivity.

Scaling relationships based on geostrophic dynamics and advective-diffusive thermal balances provide a good description of this sensitivity. The fundamental parameter describing the response of the circulation is γ, the ratio of the Sverdrup and thermal wind velocity scales. This parameter is proportional to the square root of the Ekman pumping, and inversely proportional to the cube root of the vertical diffusivity. As γ increases, the circulation is dominated by wind forcing, and takes on a multiple gyre structure. At large γ, the thermocline scale depth is set by the wind forcing at the advective scale D_a, which is independent of the vertical diffusivity. As γ decreases, the circulation consists of a single gyre with very zonal interior flow. At small γ, the thermocline scale depth is given by the diffusive scale D_d, which is proportional to the cube root of the vertical diffusivity. The same dependence on this parameter has been observed in previous sensitivity studies in which the wind forcing was varied while the vertical diffusivity was held fixed.

The enhancement of the vertical shear of the zonal flow causes the meridionally integrated zonal mass transport to increase. The transport was shown to be proportional to the product of the thermal wind velocity scale and the diffusive depth scale. The zonally integrated meridional mass transport also increases with increasing vertical diffusivity, but not to the same degree as the zonal circulation. The transition from wind forcing dominated to thermal forcing dominated circulations is also evident in the energy cycles. At small γ, there is a net conversion of kinetic to potential energy, so that the wind forcing is helping to maintain the thermocline structure. At small γ, the buoyancy work changes sign, and the thermal forcing drives a more vigorous circulation.

The poleward heat transport in this model, and other OGCMs, is dominated by the meridional overturning circulation. When a linear restoring boundary condition on the surface temperature is used, the increased meridional overturning results in a increase in the poleward heat transport. When the surface heat fluxes, and thus the poleward heat transport, are specified as boundary conditions, the sensitivity appears in the meridional and vertical temperature gradients.

This sensitivity of OGCMs is somewhat discouraging from the point of view of climate modeling. While we can expect reliable estimates of the wind stress to become available with the advent of satellite-borne instruments, the prospects for determining the vertical diffusivity are not so bright. Estimates of the magnitude of the vertical diffusivity in the ocean vary by almost two orders of magnitude. The physical processes responsible for mixing in the interior of the ocean are perhaps the most poorly understood in physical oceanography. While the horizontal resolution of the next generation of models will be adequate to resolve the

energetic eddies responsible for mixing along isopycnal surfaces, the eddies responsible for cross-isopycnal mixing have vertical scales much too small to be resolved in large-scale models. The turbulent motions responsible for cross-isopycnal (or approximately vertical mixing) will therefore continue to be parameterized for the foreseeable future.

Two of the deficiencies of the current generation of OGCMs are that the thermocline tends to be too deep, and the poleward heat transport too small. As we have seen, reducing the vertical diffusivity in order to improve the simulation of the thermocline results in a lower, and less realistic, poleward heat transport. Recent results with higher resolution models (K. Bryan, personal communication) indicate that the sensitivity of these quantities to vertical mixing is the same but that it may be possible to obtain a better overall solution. In viscous, low resolution models a very large store of available potential energy is required to drive a circulation strong enough to have a realistic poleward heat transport. Increasing the vertical diffusivity results in a larger APE supply. In models with lower dissipation, the size of the APE pool need not be as large, so it is not necessary to sacrifice the thermocline structure for realistic heat transports. Nonetheless, the sensitivity remains large and requires that we better quantify the parameterization of vertical mixing processes if we are to use ocean general circulation models as tools to investigate the role of the ocean in climate change. The results of the present study should help to provide a basis of understanding for the changes that will occur in the solutions when new mixing parameterizations are incorporated in future generations of ocean general circulation models.

Acknowledgments. This study comprised part of my doctoral dissertation, completed in the Geophysical Fluid Dynamics Program at Princeton University. I would like to thank Jorge Sarmiento, Kirk Bryan, and Syukuro Manabe for their patient and expert guidance during the course of this work. Support was provided under NSF Grant ATM8106800.

REFERENCES

Alexander, R. C., 1971: On the advective and diffusive heat balance in the interior of the subtropical ocean. *Tellus,* **23,** 393–403.

Bryan, K., 1969: A numerical method for the study of the circulation of the world ocean. *J. Comput. Phys.,* **4,** 347–376.

——, 1984: Accelerating the convergence to equilibrium of ocean-climate models. *J. Phys. Oceanogr.,* **14,** 666–673.

——, and M. D. Cox, 1967: A numerical investigation of the oceanic general circulation. *Tellus,* **19,** 54–80.

——, and ——, 1968: A numerical model of an ocean driven by wind and differential heating. Part I: Description of the three dimensional velocity and density fields. Part II: An analysis of the heat, vorticity and energy balance. *J. Atmos. Sci.,* **23,** 945–978.

——, and ——, 1972: An approximate equation of state for numerical models of the ocean circulation. *J. Phys. Oceanogr.,* **2,** 510–514.

——, and L. J. Lewis, 1979: A water mass model of the world ocean circulation. *J. Geophys. Res.,* **84,** 2503–2517.

——, and J. L. Sarmiento, 1985: Modeling ocean circulation. *Adv. Geophys.,* **28A,** 433–459.

——, S. Manabe and R. C. Pacanowski, 1975: A global ocean-atmosphere climate model. Part II: The oceanic circulation. *J. Phys. Oceanogr.,* **5,** 30–46.

Cox, M. D., 1984: A primitive equation, 3-dimensional model of the ocean. GFDL Ocean Group Tech. Rep. No. 1., GFDL/Princeton University.

——, and K. Bryan, 1984: A numerical study of the ventilated thermocline. *J. Phys. Oceanogr.,* **14,** 674–687.

Gill, A. E., and K. Bryan, 1971: Effects of geometry on the circulation of a three-dimensional southern hemisphere ocean model. *Deep-Sea Res.,* **18,** 685–721.

——, J. S. A. Green and A. J. Simmons, 1974: Energy partition in the large-scale ocean circulation and the production of mid-ocean eddies. *Deep-Sea Res.,* **21,** 499–528.

Holland, W. R., 1971: Ocean tracer distributions. *Tellus,* **23,** 371–392.

——, 1975: Energetics of baroclinic motions. *Numerical Models of the Ocean Circulation,* Natl. Acad. Sci., Washington, DC, 168–177.

Holloway, J. L., M. J. Spelman and S. Manabe, 1973: Latitude-longitude grid suitable for numerical time integration of a global atmospheric model. *Mon. Wea. Rev.,* **101,** 69–78.

Levitus, S., 1982: *Climatological Atlas Of The World Ocean,* NOAA Professional Paper 13, [Govt. Printing Office.] Washington, D.C.

Meehl, G. A., W. M. Washington and A. J. Semtner, 1982: Experiments with a global ocean model driven by observed atmospheric forcing. *J. Phys. Oceanogr.,* **12,** 301–312.

Munk, W., 1966: Abyssal recipes. *Deep-Sea Res.,* **13,** 306–318.

Semtner, A. J., 1974: An ocean general circulation model with bottom topography. *Numerical Simulation of Weather and Climate,* Tech. Rep. 9, Dept. of Meteorology, UCLA.

Takano, K., 1981: A note on the haline, thermohaline, and thermohaline-wind-driven ocean circulation. *La Mer,* **19,** 185–203.

Veronis, G., 1969: On theoretical models of the thermocline circulation. *Deep-Sea Res.,* **16**(Suppl.), 301–323.

——, 1975: The role of models in tracer studies. *Numerical Models of the Ocean Circulation,* Natl. Acad. Sci., Washington, DC, 133–146.

Welander, P., 1971: The thermocline problem. *Phil. Trans. Roy. Soc. London,* **A270,** 415–421.